Lessons Learned from Semi-Empirical Methods for the Li-Ion Battery Solid Electrolyte Interphase

Mohammed Bin Jassar, Carine Michel, Sara Abada, Theodorus de Bruin, Sylvain Tant, Carlos Nieto-Draghi, Stephan N. Steinmann

Lessons Learned from Semi-Empirical Methods for the Li-Ion Battery Solid Electrolyte Interphase

Mohammed Bin Jassar,[1,2,3] Carine Michel,[2] Sara Abada,[4] Theodorus De Bruin,[3] Sylvain Tant,[1] Carlos Nieto-Draghi,[3] and Stephan N. Steinmann[2]*

[1]Stellantis Centre Technique Carrières-sous-Poissy, 78955 Carrière-sous-Poissy, France

[2]ENS de Lyon, CNRS, Laboratoire de Chimie UMR 5182, 69364 Lyon, France

[3]IFP Energies nouvelles, 1 et 4 avenue de Bois-Préau, 92852 Rueil-Malmaison, France

[4]IFP Energies nouvelles, Rond-Point de l'échangeur de Solaize, BP 3, 69360 Solaize, France

Corresponding Author

* E-mail: stephan.steinmann@ens-lyon.fr

Abstract

Studying the chemical reactivity related to the solid electrolyte interphase (SEI) in lithium-ion batteries is challenging due to system heterogeneity (spatial and compositional). Semi-empirical methods have the potential to reduce the computational cost compared to the computationally costly DFT computations. In this study, we have first assessed the performance of four semi-empirical methods (GFN-xtb, GFN2-xtb, PM6-D3 and PM7-D3) to model major reactions for SEI formation and growth. We have included the major decomposition reactions of the most used solvent (ethylene carbonate), most used salt (lithium hexafluorophosphate) and other electrolyte species like the co-solvent 1,3-dioxolane and the additive vinylene carbonate. We have found that PM7-D3 and GFN-xtb are the two best performing methods for the 32 tested reactions. Finally, we have performed PM7-D3 and GFN-xtb -based molecular dynamics for inorganic/organic interfaces. We have found that LiF is the most rigid salt, which barely reconstructs. In contrast, Li_2O is subject to severe reconstruction at the GFN-xtb level of theory, but significantly less when using PM7-D3. Still, even at the PM7-D3 level of theory Li_2O readily reacts with alkyl carbonates, leading to CO_2 dissociation and thus the formation of surface carbonates. When in contact with ethylene carbonate, the organic molecules undergo partial dehydrogenation reactions and ring openings. This suggests that Li_2O is overly reactive to be in direct contact with such organic molecules. Rather, it is surrounded by a passivating (mono-)layer of Li_2CO_3. Indeed, our simulations suggest that such a hybrid system (core of Li_2O, shell of Li_2CO_3, solvated with ethylene carbonate) the organic solvent remains intact. Furthermore, for such a hybrid system GFN-xtb produces physically meaningful results, so that this method can be overall recommended.

1. Introduction

The solid electrolyte interphase (SEI) is a thin passivating layer formed at the anode/electrolyte interface in lithium-ion batteries as a result of the decomposition of the electrolyte by electrons from the anode[1–4]. Experimental studies were able to identify a multi-layered structure with an inorganic inner layer near the electrode/SEI interface (Li_2CO_3, LiF, and Li_2O), and an organic outer layer near the SEI/electrolyte interface consisting of alkyl carbonate, polymers, etc.[1–5]. However, due to the limitation of the experimental techniques, it is challenging to investigate other properties of the SEI like thermodynamics and kinetics of it its formation and growth[1–3,5,6]. Computational models have emerged to better understand the SEI formation and growth. Previous theoretical studies (e.g., DFT) focused on the decomposition pathways of main electrolyte species i.e., the ethylene carbonate solvent and the supporting salt lithium hexafluorophosphate, $LiPF_6$. However, due to computational cost, DFT is restricted to very short time scales and cannot model large, non-periodic systems. So, cheaper computational methods are essential to model reactions in amorphous systems like the SEI[1,2].

Reactive forcefield methods were used to study electrolyte decomposition reactions (e.g., 1,3-dioxolane[7]) and extend the simulation time. However, these reactive force fields are plagued by a difficulty of transferability: they are usually built and optimized for a specific set of reactions (e.g., the decomposition of ethylene carbonate only) and need to be reparameterized for each new composition of the system[8–10]. The limitation of reactive force fields can be traced back to the major approximations at the heart of their functional form, i.e., the inherently classical description of the chemical bonds[9,10]. Semi-empirical methods constitute a potential alternative since they are about three orders of magnitude faster than DFT. In contrast to reactive force

fields, semi-empirical methods are based on quantum mechanics and are, therefore, more transferable, i.e., less system-specific[11–14].

Semi-empirical methods are based on approximations to first principles DFT or Hartree-Fock[15–19] formalisms. One of the most successful families of the semi-empirical methods is the neglect of diatomic differential overlap methods, first introduced by John Pople[20]. Several improvements were made to the original formalism and led to the development of various flavors of Hartree-Fock-like semi-empirical methods and in particular AM1 and PM#[15–18], where popular values for # are 3, 6 and 7, referring to various generations. PM#-based methods are well established since they have regularly been updated and improved. For example, through the development of PM6, the core-core interactions were modified to use the Voityuk's core-core diatomic interaction parameters and Thiel's d-orbital approximation which led to a significant reduction in error for compounds of main-group elements and enabled its use for the whole block of the transition metals[15]. Further improvements and fixes were made to PM6 and led to the development of the most recent method among the PM# family (PM7)[16]. Unlike PM6, PM7 uses proxy functions to represent noncovalent interactions which led to improved results[16]. These semiempirical methods have been used in the literature to gain insights on systems where the use of DFT would have been computationally prohibitively expensive. For example, Rocha-Santos et al. have used PM6 and PM7 methods to gain insights into the binding energies of various ligand/protein complexes[6]. In the context of lithium-ion batteries, a study performed by Kim et al. has compared the performance of various semiempirical methods based on the Hartree-Fock methods to investigate the electronic properties of various solvents used in lithium-ion batteries[14]. They found that PM#-based methods showed better agreement with DFT reference data. Gieseking et al.[12] have also recently investigated the performance of various semi-empirical methods (PM7, PM6, PM3, AM1, MNDO) to compute formal

electrochemical redox potentials of various organic molecules. Again, PM7 was identified as the best candidate followed by PM6.

Similar to the empirically parameterized Hartree-Fock methods, approximations to DFT have been formulated which are called density functional tight binding (DFTB),[17,18,21] particularly developed in the work of Seifert, Elstner, and Frauenheim[21–27]. In contrast to PM7, which is applicable across the periodic table of the elements, in DFTB system-specific parameterizations (almost like for reactive force fields) dominate[28-30]. For example, Li et al. developed DFTB parameters for Li−Li, Li−H, Li−O, Li−C[28]. The developed parameters were used to model Li^+ desolvation and diffusion in liquid ethylene carbonate using molecular dynamics. This approach was also able to capture the effect of SEI thickness in blocking electron transfer and preventing electrolyte reduction. However, parameters for fluorinated compounds (e.g., salt $LiPF_6$) are still missing. In addition, their training set did not consider ethylene carbonate and vinyl-carbonate decomposition reaction energies, questioning their applicability to the formation of the major organic component of the SEI, i.e., alkyl carbonates. Another DFTB-based method was developed by Grimme et al.[17,18]: GFN-xtb. GFN-xtb avoids the pair-specific potentials of DFTB and, instead, uses mainly global and element-specific parameters[17]. The reduction of the pair-specific potentials has led to the need for fewer parameters and, thus, to an easier parameterization compared to DFTB[17], allowing GFN-xtb to be parameterized for all spd-block elements (Z = 1−86). Further improvements to GFN-xtb were made and led to the development of GFN2-xtb, strictly following a global and element-specific parameter strategy.[18] GFN2-xtb also uses improved terms for the multipole-extended electrostatic and exchange- correlation energy compared to its first generation. In addition, it inherently includes a newly developed dispersion correction (D4)[31,32] considering electronic structure effects that were neglected in the previously used dispersion correction (D3)[33,34] of GFN-xtb[18]. More details about these semi-empirical methods can be found in the original publications[15–18].

The assessment of the performance of semi-empirical methods to investigate various lithium-ion battery chemistries (e.g., electrolyte decomposition reactions) is still missing in the literature. With such low-cost, sufficiently accurate methods in hand (in this case PM7-D3), one could perform extensive explorations of the reactivity in the SEI, determining rate constants that could be incorporated into multi-scale, multi-physics models to enhance our atomistic understanding of the SEI growth and battery aging mechanisms. Therefore, we here perform a benchmarking study of four semi-empirical methods (GFN-xtb[17], GFN2-xtb[18], PM6-D3[15,33,34] and PM7-D3[16,33,34]) against DFT (PBE-dDsC) as a reference. DFT-based methods (e.g., PBE) are the most used methods for studying the SEI and reactions at the solid/liquid interface in general, as DFT offers the best compromise between accuracy and computational cost for large (periodic) systems. We tested the performance of the semi-empirical methods for major decomposition reactions of the most common electrolyte species used in lithium-ion batteries i.e., the most used solvent, ethylene carbonate and most used salt $LiPF_6$, together with popular additives, such as vinyl carbonate and 1,3-dioxolane[1,2,5,35–41]. The aim of the study is to investigate to which extent the semi-empirical methods can be reliable to study the reactivity in the SEI. In a second step we assess the performance of the two most accurate methods among their families (GFN-xtb and PM7-D3) for describing inorganic nanoparticles and lithium insertion into graphite. Finally, we demonstrate the capability of GFN-xtb and PM7-D3 to perform molecular dynamics (MD) calculations. The MD simulations evidence that GFN-xtb fails to describe one of the three inorganic components of the SEI (Li_2O). However, Li_2O is at the same time identified as being highly reactive at the PM7-D3 level of theory, suggesting that it is unlikely to be in direct contact with the organic solvent. Rather, it exists as a core-shell component, wrapped in a protective layer of Li_2CO_3.

2. Methods and Computational Details

All molecules were optimized using the DFT Perdew−Burke−Ernzerhof functional (GGA-PBE)[42,43] to provide reference results, to which PM6-D3, PM7-D3, GFN-xtb and GFN2-xtb are compared. The Vienna Ab initio Simulation Package VASP 5.4.4.[44–46] was exploited to run the DFT computations. Dispersion interactions were included using the density-dependent dispersion correction dDsC[47,48]. The core electrons were described using the projector augmented plane-wave (PAW) pseudopotentials. All structures were optimized using the conjugate gradient algorithm in the gas-phase. The k-point sampling of the first Brillouin zone was restricted to the Gamma point[49]. Convergence criteria were set to 10^{-6} eV and 0.03 eV/Å, for the electronic self-consistency iterations and ionic relaxation loop respectively. A Fermi smearing with a width of 0.03 eV was employed. Spin polarized calculations were performed for radical species. The cutoff energy for the plane-wave-basis was set to 600 eV. The vacuum space to avoid spurious periodic interaction was about 10 Å in all directions. The semi-empirical methods PM6[15] and PM7[50] Hamiltonians were exploited in combination with the Grimme dispersion correction D3[33,34] in Gaussian 16, revision C.01[51]. GFN-xtb computations used the standard setup in xtb version 6.4.1[17–19]. The dispersion corrections D3 and D4 are, thus, included in GFN-xtb[17] and GFN2-xtb[18] respectively. All computations were performed in vacuum (single molecule) and all energies obtained are electronic energies based on non-interacting species (without any thermodynamics corrections).

Molecular dynamics simulation

For the MD calculations, the structure of the systems was built using Packmol 20.11.0[52]. We used the hydrogen isotope tritium that allows for a step size of 1 fs without causing numerical instabilities. The MD simulations were performed for at least 10 ps. We used the ORCA software[53] to perform the GFN-xtb molecular dynamics. The temperature was set to 298 K using the Berendsen thermostat. The PM7-D3-MD simulations were performed using the atom

centered density matrix propagation molecular dynamics model (ADMP) using Gaussian16[51]. The temperature was set to 298 K relying on the built-in velocity-rescaling thermostat. The simulation time cost (system of around 550 atoms) for each 10 ps simulation (using 36 CPU cores) is around 0.5 day for GFN-xtb and 5 days for PM7-D3. We tested a similar MD system but using PBE/STO-3G using Gaussian software instead of PM7-D3. We found that it took around 5 days for only 0.17 ps. So, it would take around 290 days for 10 ps at the DFT level, highlighting the speedup obtained when using semi-empirical methods instead. Note that 10 ps are rather short, i.e., equilibration cannot be ensured. Nevertheless, trajectories of about 10 ps are found to be sufficient for qualitative insight in solid/liquid interfaces, especially when coupled with enhanced sampling[54]. The latter is, however, beyond the scope of this study.

3. Results and Discussion

3.1 Set of reactions

We evaluate the accuracy of the four semi-empirical methods, i.e., PM6-D3, PM7-D3, GFN-xtb and GFN2-xtb for 32 major (elementary) reactions that are discussed in the literature[1,2,5,35–39] of the SEI formation and growth, see Figure 1.

In terms of reactants, one can highlight Li (e.g., reaction 1), the supporting salt $LiPF_6$ (reaction 8), the solvent ethylene carbonate (reaction 12), the additive vinyl carbonate (reaction 13) and the (co-)solvent 1,3-dioxalane (reaction 29). In terms of notable products one can mention the inorganic components of the SEI Li_2O, LiF and Li_2CO_3 (reactions 1, 3 and 24, respectively) and the organic butylene and ethylene dicarbonate (reaction 25 and 27, respectively). The reaction list also includes the main decomposition reactions for the first steps in vinylene/ethylene carbonate cross polymerization reactions (e.g., reactions 18 and 22)[40] and the

reactions between 1,3-dioxolane and $LiPF_6$ (reactions 29 and 30) as reported in previous studies[7].

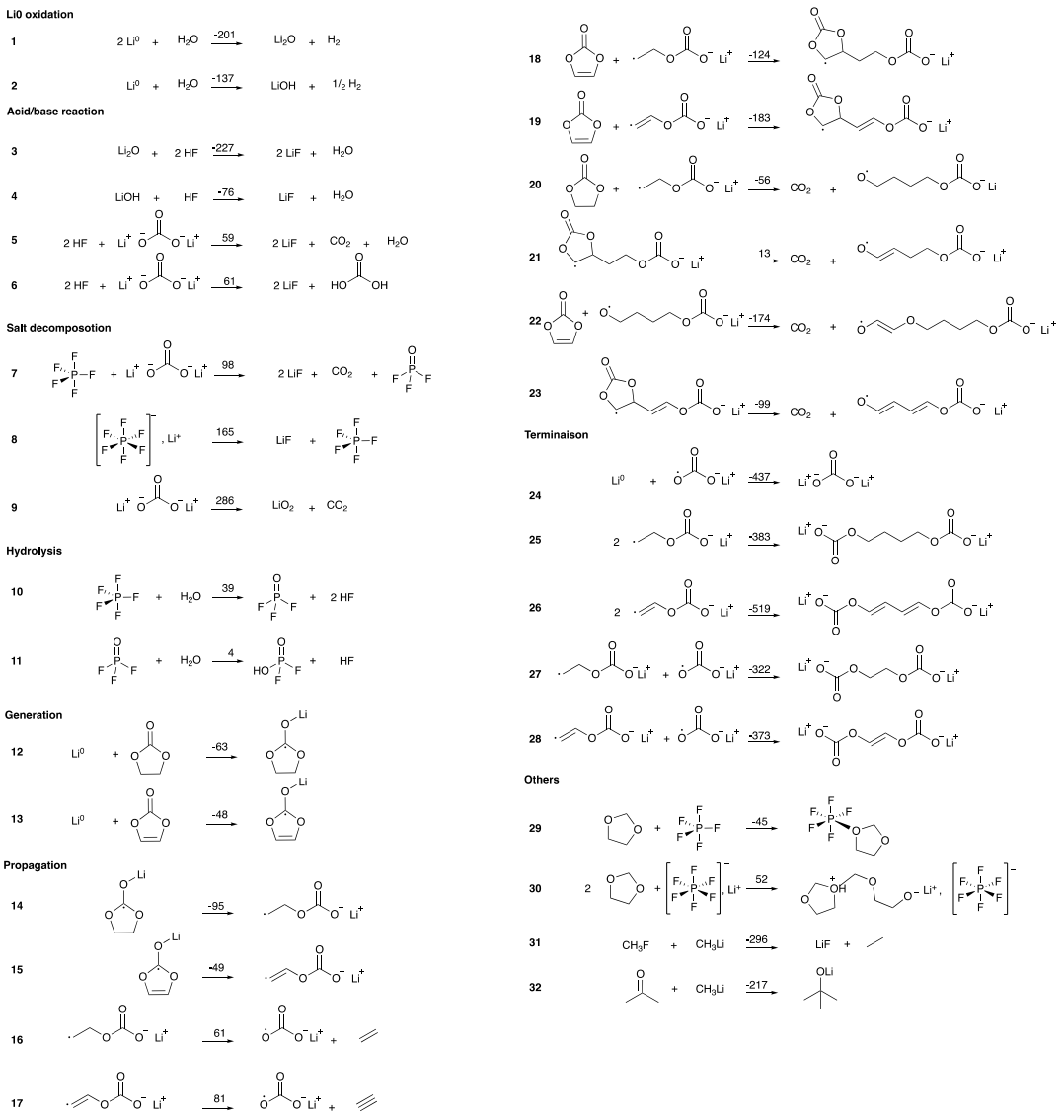

Figure 1 Reactions considered for assessing the accuracy of semi-empirical methods for reactions relevant in the context of lithium-ion batteries. Reaction energies in kJ/mol at the PBE-dDsC level of theory are indicated above the reaction arrow.

3.2 PBE-dDsC vs. Semi-Empirical Methods

To start the analysis, we investigate the overall accuracy of semi-empirical methods compared to the reference PBE-dDsC computations in Figure 2. First of all, we notice that all four tested methods lead to acceptable results in the sense that all the data is located close to the bisector, i.e., no excessive outliers have been identified. This is further confirmed by the high Pearson-correlation coefficients (R^2>0.9) for all methods. In other words, trends in relative reaction energies are quite faithfully reproduced, so that semi-empirical methods can be exploited for pre-screening of large reaction networks encountered in the SEI formation[14,55]. When considering quantitative agreement with the reference level of theory, one notices that PM6-D3 and PM7-D3 feature slopes that are closer to unity as compared to GFN-xtb and GFN2-xtb, suggesting that PM6-D3 and PM7-D3 show a smaller systematic error. Similarly, the maximum errors range from 205 kJ/mol for PM7-D3 (reaction 1) to 395 kJ/mol for GFN2-xtb (reaction 27). From this global overview, one might recommend PM6-D3 on par with PM7-D3 for use in SEI-related research. Given its high correlation coefficient, PM7-D3 is slightly preferable. This is also in line with the better performance of PM7 compared to PM6 previously reported in the literature[15,50]. For example, PM7 was found to predict more accurate geometries than PM6 for a set of 2194 solids and to feature a significant improvement in the prediction of heats of formation[15,50].

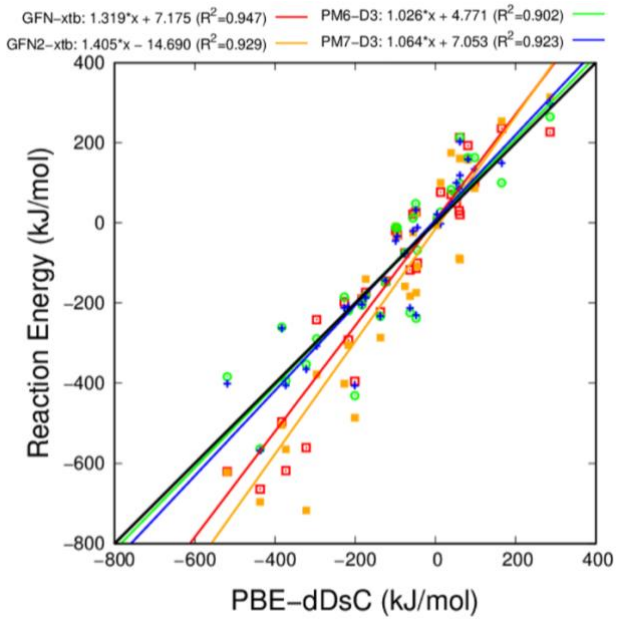

Figure 2 Parity plot for the semi-empirical methods GFN-xtb, GFN2-xtb, PM6-D3 and PM7-D3 against PBE-dDsC for all the reactions tested. The corresponding least-squares fit are given in the legend above the plot, the black diagonal line indicates the bisector.

This encouraging overall performance of semi-empirical methods has, however, to be nuanced by the consideration of the quantitative errors: Figure 3 shows the mean absolute deviations (MADs) which range from 59 kJ/mol for PM7-D3 to even 106 kJ/mol for GFN2-xtb. Similarly, the percentage deviations are above 70 % in all cases. These performance indicators demonstrate that semi-empirical methods do not yet reach quantitative agreement with DFT but should only be used for "pre-screening" purposes and/or their results need to be re-evaluated at the DFT level to achieve quantitatively reliable results.

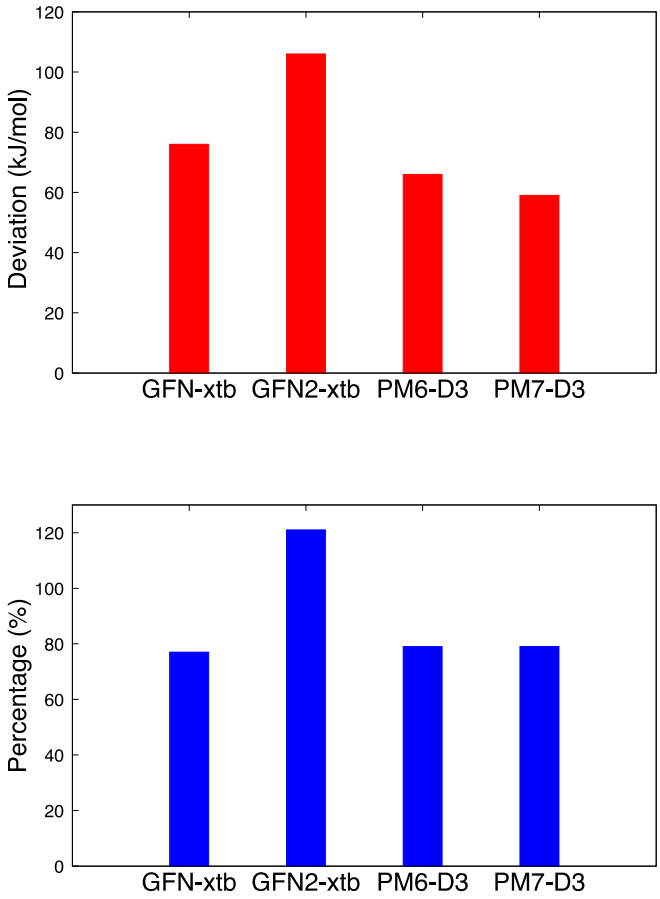

Figure 3 Top: The mean absolute deviation (MAD) and bottom the mean absolute percentage deviation for the four semi-empirical methods against PBE-dDsC.

Finally, one needs to address the question of "across-the-board" accuracy given our classification of reactions into different groups in Figure 1. Are all groups treated on an equal footing by the semi-empirical methods? This is analyzed in Figure 4. To simplify the discussion, we only show data for two out of the four tested semi-empirical methods: GFN-xtb and PM7-D3, which are the better performing variants of the two families (see SI for the corresponding graphs of the other two methods). When analyzing the MAD as a function of the reaction class, first, one notes that the two semi-empirical methods perform overall quite similarly, with two exceptions: GFN-xtb is significantly more accurate for the prediction of the reactions that generate radicals (Gen, reaction 12 and 13), while PM7-D3 is more accurate for the termination reactions (Term, reactions 24-28), suggesting that both methods are slightly imbalanced

regarding the creation/coupling of carbon-based radicals. Other than that, the oxidation of Li (LiOx, reactions 1 and 2) are badly described by both methods. One has to keep in mind, however, that these two reactions are somewhat artificial, in the sense that in the "real" SEI, the reacting Li atom is not surrounded by vacuum, but rather stabilized either as a solid (metal Li electrode) or as an intercalation compound. Furthermore, the produced LiOH and Li_2O will form solids, with electronic structures quite far from their elementary building blocks in the gas-phase.

When considering the percentage deviations, it is PM7-D3 that shows very large errors for four reactions: the two related to hydrolysis and the two related to the generation of radicals. The reason for the high relative errors is different for the two groups: The hydrolysis reactions are nearly athermic, so that even relatively small absolute errors (less than 20 kJ/mol) lead to high percentage errors, while the performance for the generation of radicals is simply bad, as already seen in the MADs. Still, GFN-xtb also shows mean percentage errors of around 100% for these reactions, so that one can conclude that these reactions are difficult to describe accurately with such low-cost methods. Table S1 and Table S2 show all reaction's energies for each method, the individual absolute % deviations and the absolute deviations relative to PBE-dDsC.

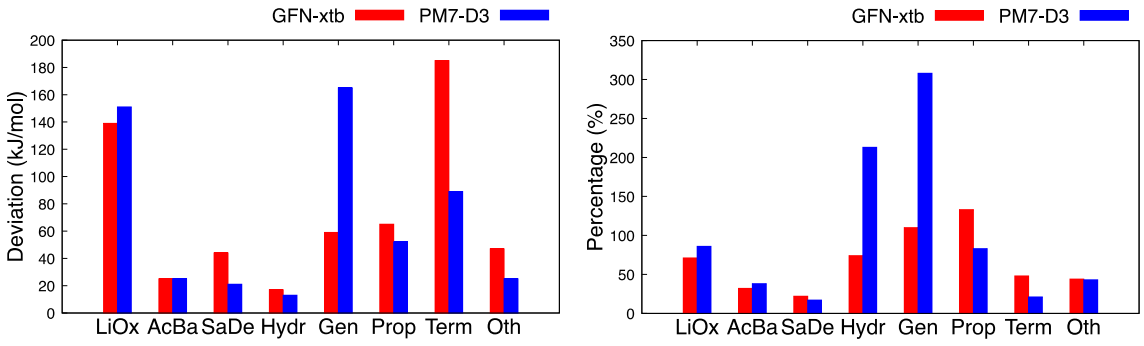

Figure 4 Left: The mean absolute deviation (MAD) and right the mean absolute percentage deviation for GFN-xtb and PM7-D3 against PBE-dDsC, reported in terms of the eight groups of reaction types defined in Figure 1.

To further check the fitness of PM7-D3 and GFN-xtb methods for computations of systems relevant to the SEI, we also need to study larger inorganic systems representing the negative electrode (in this case lithiated graphite (LiC_x)) and various salts formed from the decomposition of the main solvent and main salt: Li_2CO_3, LiF and Li_2O.

3.3 Solid components of the SEI

Lithiation of graphite

The lithiated graphite (LiC_x) is currently the most used negative electrode in lithium-ion batteries. The (de)intercalation process of Li^0 between the graphene layers is important for the cycling of the battery. In our computations, we have used two layers of graphene to host various numbers of Li^0 to mimic the battery at different degrees of lithiation, i.e., different states of charges[56], see Figure 5. These structures are inspired from the experimental[56] structures of lithiated graphite, which have been the object of a DFT benchmarking study by Lenchuk and co-workers[57]. In the first row of Figure 5, we start with a very low lithium content (LiC_{108}), where Li^0 is placed in the center between the two graphene-like layers. Increasing the Li content, we move to LiC_{36}, where three Li^0 atoms are arranged in a diagonal-like structure, in order to maximize their distances while keeping their preferred intercalation sites. Then, adding two more Li^0 atoms, one reaches again a symmetric structure. In the second row of Figure 5, we report our model for the half-lithiated electrode, which has 9 Li^0 atoms located between the graphite layers representing LiC_{12}. Finally, the fully lithiated structure features additional 9 Li atoms "on top" of the graphene sheet, leading to LiC_6.

To study the lithiation of graphite, we have computed the intercalation energy of Li atoms (following Eq.1) for the five structures described at the PBE-dDsC level of theory.

$$\text{Reaction Energy per 1 Li}^0\ \left(\frac{\text{kJ}}{\text{mol}}\right) = \frac{\text{E}_{\text{lithiated graphite}} - \text{E}_{\text{graphite}} - \text{n E}_{\text{Li}^0}}{\text{n of Li}^0} \qquad \text{Eq. (1)}$$

where n is the number of Li atoms.

Figure 5f reports the average lithiation energy as a function of the Li content. One can notice that as the number of intercalated Li^0 increases, the reaction energy per Li^0 at the PBE-dDsC level becomes slightly more exothermic (10-20 kJ/mol) until around 5 Li^0 atoms where any further addition makes the reaction energy less exothermic. The initial increase in exothermicity at low-Li contents is likely due to deformation energies: intercalating one Li^0 atom or several drives the graphitic layers to a similar extent apart. The significant decrease (40 kJ/mol) in average Li-intercalation energy going from half lithiated to fully lithiated graphite (LiC_{12} to LiC_6) has probably two origins: On one hand, in our model the "additional" layer of Li^0 is no more stabilized from both sides by carbon atoms and, on the other hand, given at least their partially positive atomic charge, the Li^0 atoms start to interact (repel) each other significantly.

The reaction energies for the lithiated graphite per 1 Li^0 atom using GFN-xtb and PM7-D3 against PBE-dDsC are shown in Figure 5f. GFN-xtb reproduces the trends excellently in comparison to PBE-dDsC for the reaction energies at the initial lithiation process (low Li^0 content). However, GFN-xtb predicted a very highly exothermic reaction energy for the fully lithiated graphite LiC_6. This high exothermicity is attributed to the fact that Li^0 atoms on the upper layer of LiC_6 aggregate to form a small cluster of Li^0 atoms, see Figure S2, indicating a failure of GFN-xtb in modeling the fully lithiated graphite (highest Li^0 content). In view of the somewhat artificial model at high Li content (no carbon layer on top), this failure of GFN-xtb is not too concerning for practical applications. Still, this qualitative failure has not been observed for PM7-D3.

Using PM7-D3, we notice that the most exothermic reaction is for Li^0 intercalation where the number of Li^0 atoms is 1 and located in the center (structure a), see Figure 5f. It should be noted that the off-set energy in Figure 5f between PM7-D3 and PBE-dDsC for the reaction energies for the lithiation of graphite is likely due to the use of the isolated Li^0 atom as a reference. Indeed, the formal oxidation of Li^0 was found to lead to significant errors according to Figure 4. In contrast to GFN-xtb, PM7-D3 follows the overall PBE-dDsC trend for high Li^0 content while the increasing exothermicity of the intercalation energy at low Li^0 content is not captured. This suggests that the deformation energy of the carbon structure is likely to be overestimated by PM7-D3, while the electrostatic repulsion between Li^0 atoms is well described.

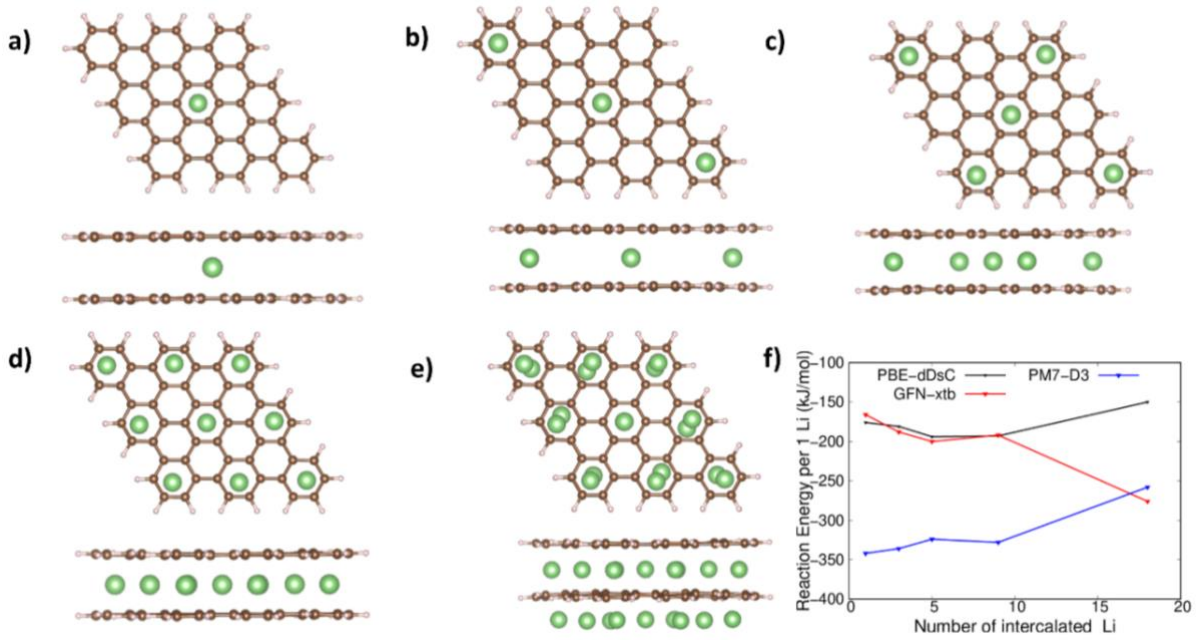

Figure 5 Representation of lithiated graphite models (a-e) and the reaction energies (kJ/mol) for the Li^0 intercalation per 1 Li^0 atom with respect to graphite and Li^0 atom (f).

SEI inorganic components: Li_2CO_3, LiF and Li_2O

The salts Li_2CO_3, LiF and Li_2O that form from the electrolyte degradation grow (from a small nanoparticle to large) with the aging of the battery and form the dense inorganic layer inside

the SEI. To check whether PM7-D3 and GFN-xtb can capture the energy changes as the nanoparticle size increases, we have built series nanoparticles of increasing size, keeping the morphology similar, see Figure 6. To quantify the growth energy, we report the relative energy of the nanoparticles normalized by the number of elementary units with respect to the largest one in the series, see Eq 2:

$$\text{Relative Energy } \left(\frac{\text{kJ}}{\text{mol}}\right) = \frac{\text{E}}{\text{n}} - \frac{\text{E}_{\text{largest nanoparticle}}}{\text{n}_{\text{largest nanoparticle}}} \qquad \text{Eq. (2)}$$

where E is the computed energy of the nanoparticle, and n is the number of molecular units.

We notice that, on one hand, GFN-xtb overestimates the relative energies in comparison to PBE-dDsC in almost all the nanoparticles (especially LiF and Li_2CO_3). On the other hand, PM7-D3 has the same trend and near quantitative agreement with PBE-dDsC and shows an overall better performance than GFN-xtb. Note that the difference in relative energies for PM7-D3 is in the order of 50 kJ/mol for the smallest nanoparticles of Li_2CO_3 and LiF (the error for Li_2O is much lower). This order of magnitude is similar to the MAD for the molecular reactions studied above, see Figure 3, indicating an overall robust and similar performance of PM7-D3 for these growth energies compared to the reaction energies studied previously.

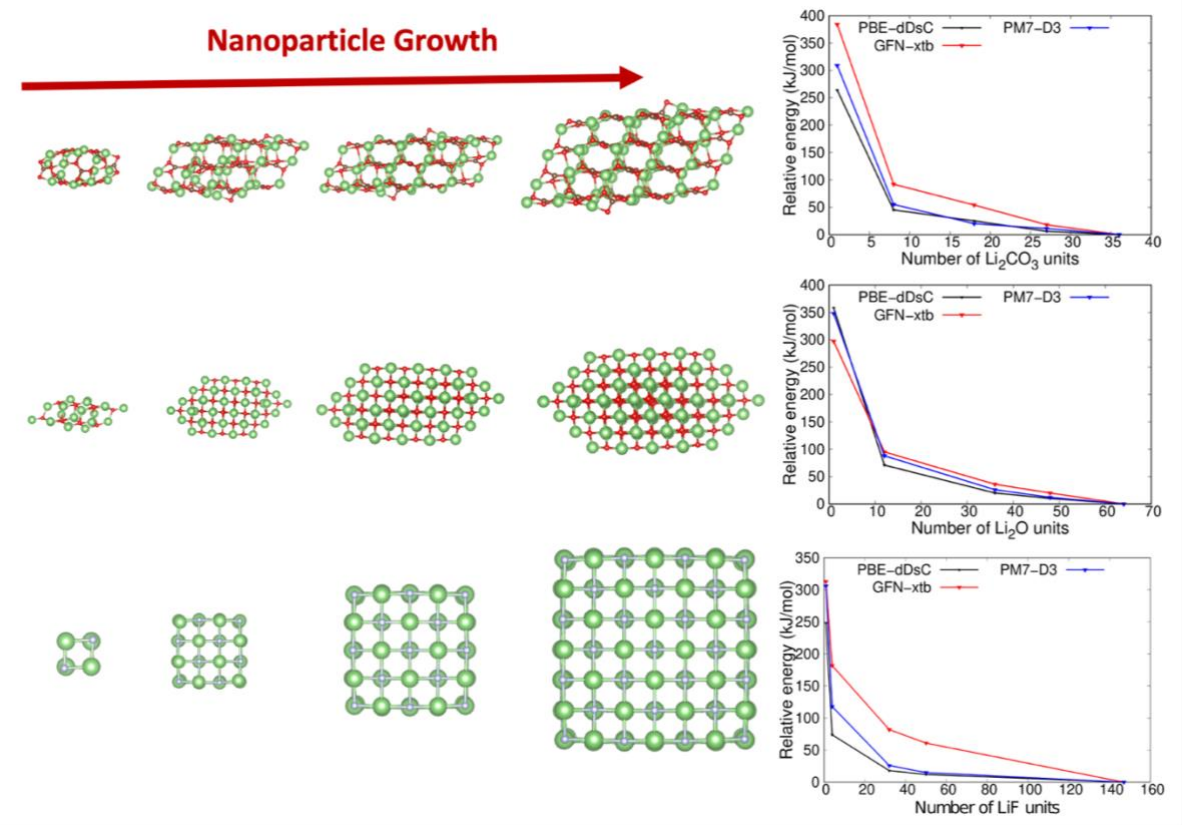

Figure 6 Left: atomic models (the smallest system included, corresponding to only one formula unit, is omitted), right graphs representing the energy for one unit of salt in a nanoparticle, relative to the corresponding energy in the largest nanoparticles as a function of the number of formula units in that particle. First row: Li_2CO_3, middle row: Li_2O, bottom: LiF. Red is O, brown is C, green is Li and light-blue is F.

3.4 Molecular Dynamics for model systems of the SEI

Structure of the inorganic nanoparticles during the molecular dynamic simulations

In this section, we will be investigating the ability of PM7-D3 and GFN-xtb to perform stable molecular dynamics simulations at 298 K. The examined systems are built based on similarly sized nanoparticles of Figure 6, representative of the inorganic components of the SEI: LiF (100

atoms representing 50 molecular unit), Li_2CO_3 (162 atoms representing 27 molecular unit) and Li_2O (108 atoms representing 36 molecular unit).

To investigate the evolution of the nanoparticles' structure over time, we have monitored the root-mean squared deviation (RMSD) with respect to the (initial) optimized geometry. The RMSD is computed using Eq.3, where N_{atoms} is the number of atoms, and $r_i(t)$ is the position of the atom i at time t.

$$\text{RMSD (Å)} = \sqrt{\frac{\sum_{i=1}^{N_{atoms}} \left(r_i(t) - r_i(0)\right)^2}{N_{atoms}}} \qquad \text{Eq. (3)}$$

The evolution of the RMSD over the MD trajectory for the isolated nanoparticles (Li_2CO_3, Li_2O and LiF) using PM7-D3 are shown in Figure 7, and the corresponding data for GFN-XTB is shown in Figure S2. We notice that the RMSD for Li_2CO_3 and Li_2O increase over time which indicates a reconstruction, especially for Li_2CO_3, where the RMSD reaches about 2 Å. For Li_2CO_3, the carbonates at the edges reorient it to form a semispherical structure while for Li_2O the nanoparticle experienced a more random movement of atoms while maintaining the overall structure integrity. We remind the reader that the initial shape of these nanoparticles is built based on rough estimates on how to cleave the bulk to expose a majority of low-energy index surfaces, while keeping the bulk stoichiometry and a similar shape for different sizes. Hence, the larger mobility of Li_2CO_3 compared to Li_2O might not only reflect a lower cohesive energy, but may also result from reconstructions to lower the surface (free) energies. In contrast, LiF, which is here represented as an ideal "cube", i.e., with a shape in close agreement with an ideal Wulff construction shape, has the lowest RMSD (around 0.25 Å) indicating a rigid structure. These contrasting trends are also seen in the evolution of the potential energy as a function of the simulation time (Fig. S4): LiF shows only small fluctuations once it has been thermalized and Li2O shows a small stabilization during the first ps and then a very small drift over the

remaining 9 ps. For lithium carbonate, however, there is a very strong stabilization during the first 5 ps after which the nanoparticle seems to have reached an equilibrium. The formation of a rigid inorganic layer (i.e., LiF) in the SEI is crucial to stabilize the battery, prevent dendrite formation and reduces capacity loss. The here observed rigidity of LiF could rationalize the general use of fluorinated salts in the electrolyte to form a stable SEI. Still, the rigidity of LiF is a double-edged sword, as it could also prevent Li diffusion.

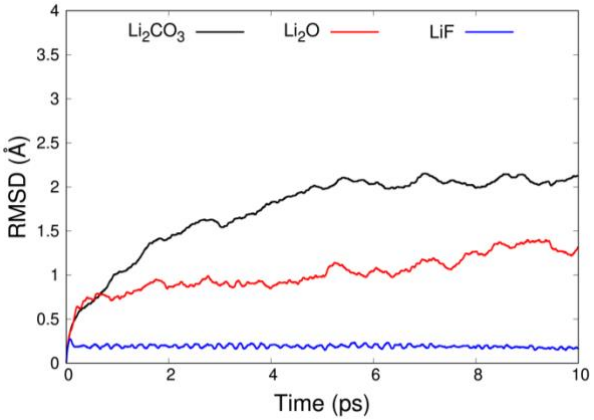

Figure 7 The values of the root-mean squared deviation (RMSD) over time obtained from the molecular dynamics' simulation using PM7-D3 for the isolated nanoparticles.

Using GFN-xtb to perform the molecular dynamics of the isolated nanoparticles, LiF and Li_2CO_3 behave similarly to the PM7-D3 simulations, see Figure S3 for details. This indicates robust performance and chemically reasonable results for these inorganic compounds. However, GFN-xtb failed to maintain the crystalline structure of Li_2O: the nanoparticle severely reconstructs. This reconstruction is also visible in the potential energy as a function of simulation time (see Fig. S4): Li_2O simulated with GFN-xtb shows a clear drift towards lower energies as a function of time and would ultimately reach a structure that could be expected to reach a lower energy than the starting point. While less pronounced, the evolution of the potential energy for Li_2CO_3 also indicates a stabilizing reconstruction, in agreement with the observations at the PM7-D3 level of theory. Surprisingly, the nanoparticle does not even get

consistently more compact: since some "voids" are created during the MD, see Figure 8. Given the ionic nature of Li_2O, such voids are deemed physically unsound and indicative of a miss-balance between isotropic ionic interactions and directional orbital interactions. This strong geometric deformation during the MD using GFN-xtb was also reflected in a notably higher RMSD values over time in comparison to PM7-D3 (reaching 2.0 Å vs 1.3 Å), see Figure S2. Still, monitoring the average coordination number of Li, as obtained by the parameter-free anisotropically corrected solid-angle nearest neighbor algorithm,[58] shows very small differences, both between PM7-D3 and GFN-xtb, but also between the three salts: The average coordination number hovers between 4 and 4.5 (see Figure S5), while the standard deviation of the coordination number for a given structure is around 1.5. This shows that the local structure around Li is not discriminating. Thus, and following our overall assessment up to this point, we recommend the rather robust PM7-D3 to investigate the chemistry of SEI.

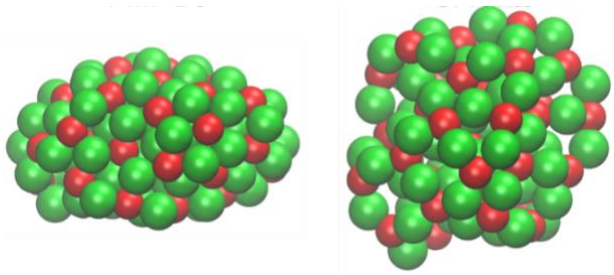

Figure 8 Final configuration of Li_2O after 10 ps PM7-D3 (left) and GFN-xtb (right), corresponding to an RMSD of 1.3 Å and 2.0 Å, respectively.

Inorganic/organic interfaces

The detailed investigation of inorganic/organic interfaces is a major challenge not only experimentally but also, computationally when using DFT due to the system size. Hence, getting rapid access to the characterization and reactivity of these interfaces via semi-empirical methods leads to insights that are difficult to obtain otherwise. We have constructed nine

prototypical inorganic/organic interfaces via the combination of the three inorganic nanoparticles studied above (Li_2O, Li_2CO_3 and LiF) and three organic phases: the solvent ethylene carbonate and the two main constituents of the organic SEI, butylene and ethylene dicarbonates. Figure 9 shows a screenshot of each of the 9 hybrid systems obtained after 10 ps of PM7-D3 simulation at 298 K.

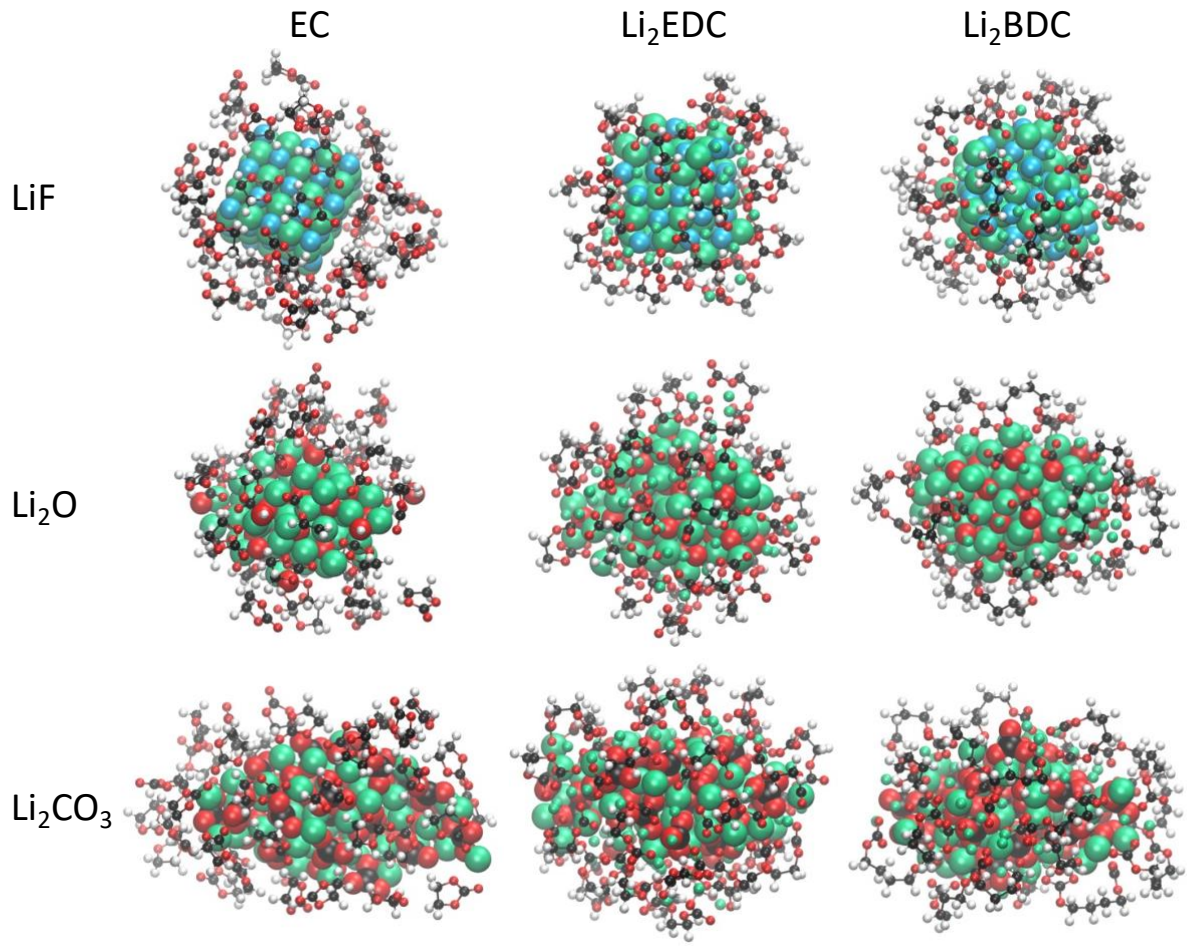

Figure 9 Screenshots after 10 ps of PM7-D3 molecular dynamics of all the nanoparticles (LiF, Li_2O and Li_2CO_3) surrounded by Li_2EDC, Li_2BDC and EC): white is H, red is O, brown is C, green is Li and light-blue is F. The atoms originating from the nanoparticles are represented in large spheres, while the organic component is represented in ball and sticks. In other words, the small green balls are Li^+ stemming from the organic compound.

For the inorganic/alkyl carbonate interfaces where the alkyl carbonates surround the nanoparticles (LiF and Li_2CO_3), we notice that the alkyl carbonates form a cation-connected network, with some of the carbonate functional groups being bound to the lithium ions of the inorganic phase, see Figure 9. These disordered structures on top of the inorganic components could explain the uncertainty in identifying the precise nature of the inorganic/organic interface in the SEI[1,2,5]. Ethylene carbonate adsorbs mainly through its carbonate functional group, in general nearly parallel to the surface, see Figure 9. It should be noted that after 10 ps of simulations (including thermalization, see computational details) we did not notice any reactions between the nanoparticles LiF and Li_2CO_3, and either ethylene carbonate or the alkyl carbonates (Li_2EDC/Li_2BDC).

In contrast to LiF and Li_2CO_3, Li_2O showed high reactivity with all the organic molecules. When surrounding Li_2O by Li_2EDC or Li_2BDC, we noticed C-O dissociations of one of the carbonate groups in Li_2EDC/Li_2BDC which led to formation of CO_2. Combined with a surface oxygen atom, it yields to carbonate adsorbed on the Li_2O surface. Figure 10 shows the C-O bond distance of the carbonate fragments of some molecules of Li_2EDC and Li_2BDC. For example, for Li_2EDC, the initial C-O bond length is around 1.4 Å and the first C-O scission occurs already after around 1.1 ps. This high reactivity of Li_2O nanoparticle is attributed to the high reactivity of the oxygen atom over the surface.

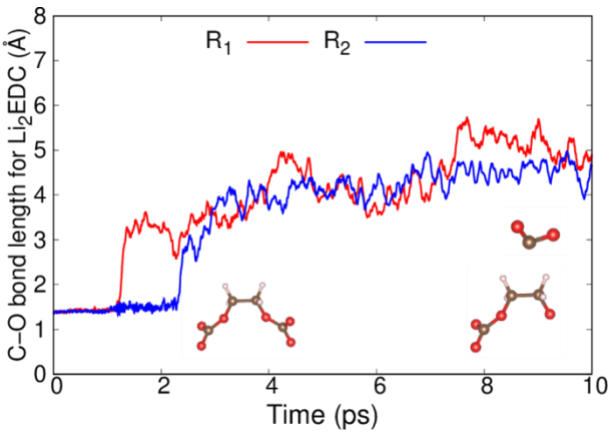

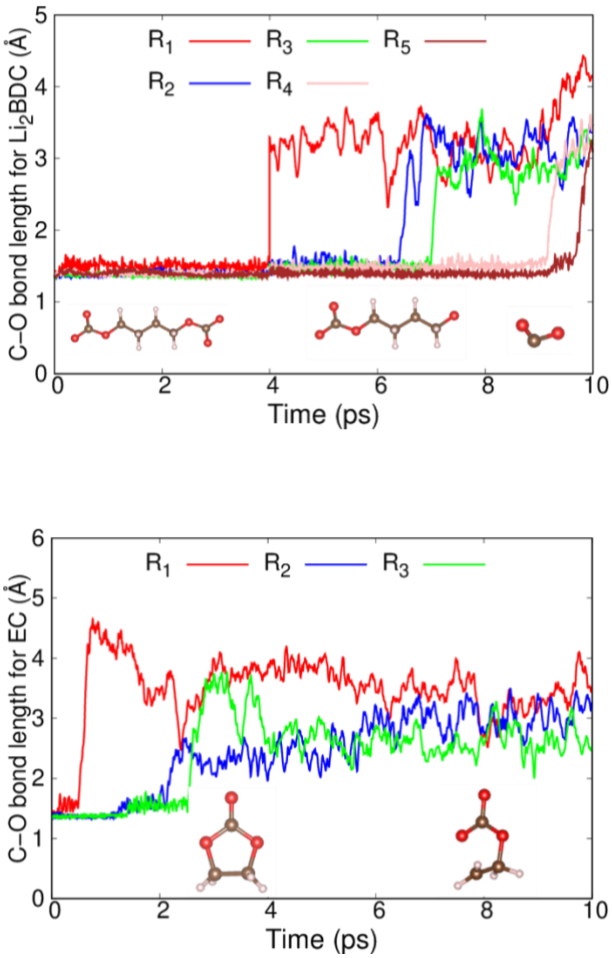

Figure 10 Reactive events observed during 10 ps of PM7-D3 molecular dynamics of a Li_2O nanoparticle in contact with an organic layer. C-O bond length distance for Li_2EDC (top) and Li_2BDC (middle) and EC (bottom). R_n represents the chemical reaction: for Li_2EDC and Li_2BDC (CO_2 dissociation reaction) while for EC we monitor the ring opening reaction. n represent the n^{th} reactive molecule.

For the system where the ethylene carbonate molecules surround Li_2O, we noticed that some of the ethylene carbonate molecules undergo a ring opening reaction through the breaking of the C-O bond. Figure 10 shows the C-O bond length of three ethylene carbonate molecules over Li_2O. The initial bond length is around 1.4 Å. The first ring opening (C-O scission) occurs already after 0.5 ps, with the carbonyl carbon atom reforming a carbonate with a surface oxygen atom. For this first ring opening, the ethylene carbonate was already in the vicinity (3.2 Å) of

the reactive oxygen in Li_2O at the beginning of the molecular dynamic simulation. However, the second and third ring-opening reactions start only when the second and the third EC molecules get closer to the oxygen in Li_2O (starting from around 2.2 and 2.8 ps respectively). This ring-opening reaction of EC over the Li_2O nanoparticle provides an alternative path for the decomposition reaction in addition to the conventional path where EC reacts with Li^0 (reaction 14 in Figure 1). It should be noted that in addition to EC ring opening reaction, we also noticed a C-H scission for some EC (closed and opened) molecules leading to the formation of inorganic OH. The resulting radical either undergoes subsequent ring-opening or is in close contact (2.2 to 2.4 Å) with lithium ions. This hydrogen atom transfer reduces the reactivity of the oxygen atoms on the surface of Li_2O and parallels the experimental reports of OH species in the inorganic component of SEI[1,2,4]. Furthermore, this observation of a C-H scission in EC suggests a possible path towards vinylene carbonate if a second dehydrogenation occurred, an event that has not been captured in our 10 ps MDs. The *in situ* formation of vinylene carbonate could rationalize the low amounts of vinylene carbonate that are specifically added to the electrolyte in commercial lithium batteries.

To test the robustness of the PM7-D3 molecular dynamics and to assess whether reactions (e.g., ring-opening of EC) occurs systematically, we have decreased the temperature of the MD to 100 K. Again, we have observed ring opening events over the Li_2O. It should be noted that the high reactivity of Li_2O solid was previously mentioned in the literature:[59] in an ab initio MD to investigate effect of the SEI on the reactivity of polysulfide over Li-metal anode, Bertolini et al. found that Li_2O is the most reactive salt compared to LiF and Li_3N which leads to the decomposition of lithium polysulfides found in the electrolyte of Li-S batteries[59]. To further investigate the reactivity of Li_2O nanoparticle, we have also performed a GFN-xtb MD for the same system (EC molecules surrounding the Li_2O nanoparticle). Even though the geometrical integrity of Li_2O is lost with GFN-xtb, the observed chemical reactivity is very similar to PM7-

D3, i.e., the ring-opening and the deprotonation of ethylene carbonate is reproduced. The fact that both of these methods capture this somewhat unexpected reactivity strongly indicates that the oxygen atoms at the Li_2O surface are "overly" reactive. In other words, Li_2O is unlikely to exist in direct contact with the ethylene carbonate solvent. Rather, we suggest that the formation of Li_2O from Li_2CO_3 is incomplete, i.e., we would expect core (Li_2O)/shell (Li_2CO_3) structures.

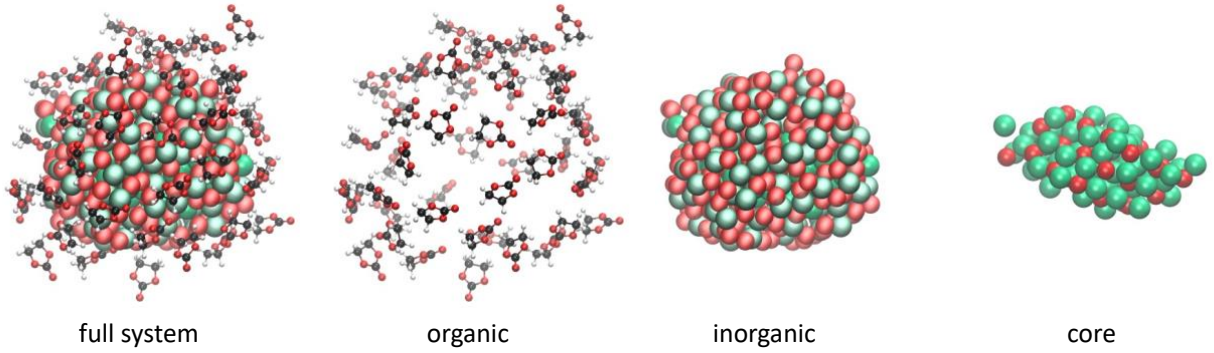

Figure 11: Core Li_2O surrounded by inorganic Li_2CO_3 and ethylene carbonate solvent molecules after 10 ps of MD at 298 K at the GFN-xtb level of theory.

To ascertain the passivating nature of Li_2CO_3, we have built a system with a nanoparticle composed of a Li_2O core, surrounded by an amorphous (mono-)layer (few Å thick, see Figure 11) of Li_2CO_3. Then, we solvated this nanoparticle with ethylene carbonate to investigate the reactivity of this hybrid system, leading to a total system size of about 1100 atoms. For technical reasons related to their implementations, the PM7-D3 simulations turned out to be significantly slower than GFN-xtb for this system size (we estimated 40 days on 36 CPUs, vs 6 days on 8 CPUs). Given that the reactivity observed with GFN-xtb was qualitatively the same to the one obtained with PM7-D3, we have used GFN-xtb to run this final simulation. In order to equilibrate the Li_2CO_3 shell around the Li_2O core, the latter was kept frozen for the first 10 ps. After additional 10 ps of completely free MD, we still did not notice any reactions, indicating

that the reactivity of Li_2O is well passivated by Li_2CO_3 and the final arrangement of the system is shown in Figure 11. It is noteworthy that, at least on the time-scale of the present simulations, the carbonate shell has also stabilized the structural integrity (RMSD of about 1 Å) of the Li_2O core, even at the GFN-xtb level of theory, independently on the presence or not of the solvating ethylene carbonate, see Figure S6.

4. Conclusion

We have performed a benchmark study of the performance of the semi-empirical methods: GFN-xtb, GFN2-xtb, PM6-D3 and PM7-D3 against PBE-dDsC to model major solid electrolyte interphase (SEI) reaction in lithium-ion batteries. We have investigated a set of 32 reactions based on the literature including the decomposition of major electrolyte species of the main solvent ethylene carbonate, the most used salt lithium hexafluorophosphate, the additive vinylene carbonate and the (co-)solvent 1,3-dioxolane. We found that PM7-D3 is the most accurate low-cost model, with a mean absolute deviation 59 kJ/mol, even though this method fails to predict the generation of organic radicals quantitatively. In terms of percentage deviations and correlation coefficient, GFN-xtb is slightly more accurate than PM7-D3. For GFN-xtb, radical termination reactions are prone to the largest errors. We have then performed further computations to assess the performance of PM7-D3 and GFN-xtb to model larger (solid) systems: lithiated graphite (LiC_x) and inorganic salt nanoparticles. We found that PM7-D3 is in qualitative agreement with PBE-dDsC for the lithiation, while GFN-xtb is in excellent agreement except at the highest Li content. Furthermore, GFN-xtb and PM7-D3 both capture qualitatively the effect of the size of the nanoparticles, with PM7-D3 reaching near quantitative agreement. Finally, we have performed 10 ps molecular dynamics at the PM7-D3 and GFN-xtb level of theory for the inorganic/organic interfaces typical for the SEI. We evidence CO_2 dissociation of alkyl carbonates and ring opening reactions along with dehydrogenation

reactions of ethylene carbonate in contact with Li_2O. Hence, our study demonstrates a significantly higher reactivity of Li_2O as compared to LiF and Li_2CO_3. Nevertheless, a very thin layer of Li_2CO_3 has been found to be sufficient to passivate Li_2O. In other words, our simulations show that Li_2O is unlikely to be in direct contact with the organic solvent, as the latter would immediately react, leading to decomposition products such as OH, carbonates and potentially vinylene carbonate, a common additive in Li-ion batteries.

ASSOCIATED CONTENT

The Supporting Information is available free of charge on the ACS Publication website at DOI:

Further information is available on all reaction's energies for each method and the individual absolute % deviations and absolute deviations relative to PBE-dDsC.

The geometries of all reactions and solid structures (lithiated graphite and nanoparticles) obtained from the DFT (PBE-dDsC) calculations can be found on nomad-lab.eu. See DOI: 10.17172/NOMAD/2023.06.20-1.

Acknowledgement

This work was supported by the program Convention, Industrielle de Formation par la Recherche (CIFRE) N° 2020/0918 of the Association Nationale de la Recherche et, de la Technologie (ANRT). The authors thank the SYSPROD project and AXELERA Pôle de Compétitivité for financial support (PSMN Data Center).

References

(1) Wang, A.; Kadam, S.; Li, H.; Shi, S.; Qi, Y. Review on modeling of the anode solid electrolyte interphase (SEI) for lithium-ion batteries. npj Comput Mater 2018, 4 (1), 15. DOI: 10.1038/s41524-018-0064-0.

(2) Franco, A. A.; Rucci, A.; Brandell, D.; Frayret, C.; Gaberscek, M.; Jankowski, P.; Johansson, P. Boosting Rechargeable Batteries R&D by Multiscale Modeling: Myth or Reality? Chem. Rev 2019, 119 (7), 4569–4627. DOI: 10.1021/acs.chemrev.8b00239.

(3) Abada, S. ; Marlair, G.; Lecocq, A.; Petit, M.; V. Sauvant-Moynot; F. Huet. Safety focused modeling of lithium-ion batteries: A review. J. Power Sources 2016, 306, 178–192. DOI: 10.1016/j.jpowsour.2015.11.100.

(4) Franco, A. A. Multiscale modelling and numerical simulation of rechargeable lithium ion batteries: concepts, methods and challenges. RSC Adv. 2013, 3 (32), 13027. DOI: 10.1039/c3ra23502e.

(5) Spotte-Smith, E. W. C.; Kam, R. L.; Barter, D.; Xie, X.; Hou, T.; Dwaraknath, S.; Blau, S. M.; Persson, K. A. Toward a Mechanistic Model of Solid–Electrolyte Interphase Formation and Evolution in Lithium-Ion Batteries. ACS Energy Lett. 2022, 7 (4), 1446–1453. DOI: 10.1021/acsenergylett.2c00517..

(6) Rocha-Santos, A.; Chaves, E. J. F.; Grillo, I. B.; Freitas, A. S. de; Araújo, D. A. M.; Rocha, G. B. Thermochemical and Quantum Descriptor Calculations for Gaining Insight into Ricin Toxin A (RTA) Inhibitors. ACS omega 2021, 6 (13), 8764–8777. DOI: 10.1021/acsomega.0c02588.

(7) M. Xie; Y. Wu; Y. Liu; P.P. Yu; R. Jia; W.A. Goddard; T. Cheng. Pathway of in situ polymerization of 1,3-dioxolane in LiPF6 electrolyte on Li metal anode. Mater. Today Energy 2021, 21, 100730. DOI: 10.1016/j.mtener.2021.100730.

(8) Bedrov, D.; Smith, G. D.; van Duin, A. C. T. Reactions of singly-reduced ethylene carbonate in lithium battery electrolytes: a molecular dynamics simulation study using the ReaxFF. J. Phys. Chem. A 2012, 116 (11), 2978–2985. DOI: 10.1021/jp210345b.

(9) Islam, M. M.; van Duin, A. C. T. Reductive Decomposition Reactions of Ethylene Carbonate by Explicit Electron Transfer from Lithium: An eReaxFF Molecular Dynamics Study. J. Phys. Chem. C 2016, 120 (48), 27128–27134. DOI: 10.1021/acs.jpcc.6b08688.

(10) Islam, M. M.; Kolesov, G.; Verstraelen, T.; Kaxiras, E.; van Duin, A. C. T. eReaxFF: A Pseudoclassical Treatment of Explicit Electrons within Reactive Force Field Simulations. J. Chem. Theory Comput 2016, 12 (8), 3463–3472. DOI: 10.1021/acs.jctc.6b00432.

(11) Dral, P. O.; Wu, X.; Spörkel, L.; Koslowski, A.; Thiel, W. Semiempirical Quantum-Chemical Orthogonalization-Corrected Methods: Benchmarks for Ground-State Properties. J. Chem. Theory Comput 2016, 12 (3), 1097–1120. DOI: 10.1021/acs.jctc.5b01047.

(12) Gieseking, R. L. M.; Ratner, M. A.; Schatz, G. C. Benchmarking Semiempirical Methods To Compute Electrochemical Formal Potentials. J. Phys. Chem. A 2018, 122 (33), 6809–6818. DOI: 10.1021/acs.jpca.8b05143.

(13) Zhou, X.; Khetan, A.; Er, S. Evaluation of Computational Chemistry Methods for Predicting Redox Potentials of Quinone-Based Cathodes for Li-Ion Batteries. Batteries 2021, 7 (4), 71. DOI: 10.3390/batteries7040071.

(14) Daejin Kim; Hyein Guk; Seung-Hoon Choi; Dong Hyen Chung. Benchmarking of computational approaches for fast screening of lithium ion battery electrolyte solvents. Chem. Phys. Lett.2017, 681, 64–68. DOI: 10.1016/j.cplett.2017.05.062.
(15) Stewart, J. J. P. Optimization of parameters for semiempirical methods V: modification of NDDO approximations and application to 70 elements. J. Mol. Model. 2007, 13 (12), 1173–1213. DOI: 10.1007/s00894-007-0233-4.
(16) Stewart, J. J. P. Optimization of parameters for semiempirical methods VI: more modifications to the NDDO approximations and re-optimization of parameters. J. Mol. Model. 2013, 19 (1), 1–32. DOI: 10.1007/s00894-012-1667-x.
(17) Grimme, S.; Bannwarth, C.; Shushkov, P. A Robust and Accurate Tight-Binding Quantum Chemical Method for Structures, Vibrational Frequencies, and Noncovalent Interactions of Large Molecular Systems Parametrized for All spd-Block Elements (Z = 1-86). J. Chem. Theory Comput 2017, 13 (5), 1989–2009. DOI: 10.1021/acs.jctc.7b00118.
(18) Bannwarth, C.; Ehlert, S.; Grimme, S. GFN2-xTB-An Accurate and Broadly Parametrized Self-Consistent Tight-Binding Quantum Chemical Method with Multipole Electrostatics and Density-Dependent Dispersion Contributions. J. Chem. Theory Comput 2019, 15 (3), 1652–1671. DOI: 10.1021/acs.jctc.8b01176.
(19) Bannwarth, C.; Caldeweyher, E.; Ehlert, S.; Hansen, A.; Pracht, P.; Seibert, J.; Spicher, S.; Grimme, S. Extended tight-binding quantum chemistry methods. WIREs Comput Mol Sci 2021, 11 (2), e1493. DOI: 10.1002/wcms.1493.
(20) Pan, Y. K. Approximate molecular orbital theory (Pople, John A.; Beveridge, David L.). J Chem. Educ.1971, 48 (2), A116. DOI: 10.1021/ed048pA116.1.
(21) Gaus, M.; Cui, Q.; Elstner, M. DFTB3: Extension of the self-consistent-charge density-functional tight-binding method (SCC-DFTB). J. Chem. Theory Comput 2012, 7 (4), 931–948. DOI: 10.1021/ct100684s.
(22) Cui, Q.; Elstner, M.; Kaxiras, E.; Frauenheim, T.; Karplus, M. A QM/MM Implementation of the Self-Consistent Charge Density Functional Tight Binding (SCC-DFTB) Method. J. Phys. Chem. B 2001, 105 (2), 569–585. DOI: 10.1021/jp0029109.
(23) Elstner, M.; Porezag, D.; Jungnickel, G.; Elsner, J.; Haugk, M.; Frauenheim, T.; Suhai, S.; Seifert, G. Self-consistent-charge density-functional tight-binding method for simulations of complex materials properties. Phys. Rev. B 1998, 58 (11), 7260–7268. DOI: 10.1103/PhysRevB.58.7260.
(24) Gaus, M.; Cui, Q.; Elstner, M. Density functional tight binding: application to organic and biological molecules. WIREs Comput Mol Sci 2014, 4 (1), 49–61. DOI: 10.1002/wcms.1156.
(25) Niehaus, T. A.; Suhai, S.; Della Sala, F.; Lugli, P.; Elstner, M.; Seifert, G.; Frauenheim, T. Tight-binding approach to time-dependent density-functional response theory. Phys. Rev. B 2001, 63 (8), 85108. DOI: 10.1103/PhysRevB.63.085108.
(26) Thomas Frauenheim; Gotthard Seifert; Marcus Elstner; Thomas Niehaus; Christof Köhler; Marc Amkreutz; Michael Sternberg; Zoltán Hajnal; Aldo Di Carlo; Sándor Suhai. Atomistic simulations of complex materials: ground-state and excited-state properties. , J. Phys. Condens. Matter. 2002, 14 (11), 3015. DOI: 10.1088/0953-8984/14/11/313.
(27) Yang, Y.; Yu, H.; York, D.; Cui, Q.; Elstner, M. Extension of the self-consistent-charge density-functional tight-binding method: third-order expansion of the density functional theory

total energy and introduction of a modified effective coulomb interaction. J. Phys. Chem. A 2007, 111 (42), 10861–10873. DOI: 10.1021/jp074167r.
(28) Li, Y.; Qi, Y. Transferable Self-Consistent Charge Density Functional Tight-Binding Parameters for Li–Metal and Li-Ions in Inorganic Compounds and Organic Solvents. J. Phys. Chem. C 2018, 122 (20), 10755–10764. DOI: 10.1021/acs.jpcc.8b01839.
(29) Kubař, T.; Bodrog, Z.; Gaus, M.; Köhler, C.; Aradi, B.; Frauenheim, T.; Elstner, M. Parametrization of the SCC-DFTB Method for Halogens. J. Chem. Theory Comput. 2013, 9, 2939– 2949, DOI: 10.1021/ct4001922
(30) Gaus, M.; Goez, A.; Elstner, M. Parametrization and Benchmark of DFTB3 for Organic Molecules. J. Chem. Theory Comput. 2013, 9, 338– 354, DOI: 10.1021/ct300849w
(31) Caldeweyher, E.; Bannwarth, C.; Grimme, S. Extension of the D3 dispersion coefficient model. J. Chem. Phys. 2017, 147 (3), 034112. DOI: 10.1063/1.4993215.
(32) Caldeweyher, E.; Mewes, J.-M.; Ehlert, S.; Grimme, S. Extension and evaluation of the D4 London-dispersion model for periodic systems. Phys. Chem. Chem. Phys. 2020, 22 (16), 8499–8512. DOI: 10.1039/d0cp00502a.
(33) Grimme, S.; Antony, J.; Ehrlich, S.; Krieg, H. A consistent and accurate ab initio parametrization of density functional dispersion correction (DFT-D) for the 94 elements H-Pu. J. Chem. Phys. 2010, 132 (15), 154104. DOI: 10.1063/1.3382344.
(34) Grimme, S.; Ehrlich, S.; Goerigk, L. Effect of the damping function in dispersion corrected density functional theory. J. Comput. Chem. 2011, 32 (7), 1456–1465. DOI: 10.1002/jcc.21759.
(35) Spotte-Smith, E. W. C.; Petrocelli, T. B.; Patel, H. D.; Blau, S. M.; Persson, K. A. Elementary Decomposition Mechanisms of Lithium Hexafluorophosphate in Battery Electrolytes and Interphases. ACS Energy Lett. 2023, 8 (1), 347–355. DOI: 10.1021/acsenergylett.2c02351.
(36) Grugeon, S.; Jankowski, P.; Cailleu, D.; Forestier, C.; Sannier, L.; Armand, M.; Johansson, P.; Laruelle, S. Towards a better understanding of vinylene carbonate derived SEI-layers by synthesis of reduction compounds. J. Power Sources 2019, 427, 77–84. DOI: 10.1016/j.jpowsour.2019.04.061.
(37) Wang, Y.; Nakamura, S.; Tasaki, K.; Balbuena, P. B. Theoretical studies to understand surface chemistry on carbon anodes for lithium-ion batteries: how does vinylene carbonate play its role as an electrolyte additive? J. Am. Chem. Soc.2002, 124 (16), 4408–4421. DOI: 10.1021/ja017073i.
(38) Wang, Y.; Nakamura, S.; Ue, M.; Balbuena, P. B. Theoretical studies to understand surface chemistry on carbon anodes for lithium-ion batteries: reduction mechanisms of ethylene carbonate. J. Am. Chem. Soc. 2001, 123 (47), 11708–11718. DOI: 10.1021/ja0164529.
(39) Abbott, J. W.; Hanke, F. Kinetically Corrected Monte Carlo-Molecular Dynamics Simulations of Solid Electrolyte Interphase Growth. J. Chem. Theory Comput 2022, 18 (2), 925–934. DOI: 10.1021/acs.jctc.1c00921.
(40) Kuai, D.; Balbuena, P. B. Solvent Degradation and Polymerization in the Li-Metal Battery: Organic-Phase Formation in Solid-Electrolyte Interphases. ACS Appl. Mater. Interfaces 2022, 14 (2), 2817–2824. DOI: 10.1021/acsami.1c20487.
(41) Bin Jassar, M.; Michel, C.; Abada, S.; Bruin, T. de; Tant, S.; Nieto-Draghi, C.; Steinmann, S. N. A Joint DFT-kMC Study To Model Ethylene Carbonate Decomposition Reactions: SEI

Formation, Growth, and Capacity Loss during Calendar Aging of Li-Metal Batteries. ACS Appl. Energy Mater. 2023, 6 (13), 6934–6945. DOI: 10.1021/acsaem.3c00372.
(42) Perdew, J. P.; Burke, K.; Ernzerhof, M. Generalized Gradient Approximation Made Simple. Phys. Rev. Lett. 1996, 77 (18), 3865–3868. DOI: 10.1103/PhysRevLett.77.3865.
(43) Perdew, J. P.; Burke, K.; Ernzerhof, M. Generalized Gradient Approximation Made Simple [Phys. Rev. Lett. 77, 3865 (1996)]. Phys. Rev. Lett. 1997, 78 (7), 1396. DOI: 10.1103/PhysRevLett.78.1396.
(44) Kresse, G.; Furthmüller, J. Efficient iterative schemes for ab initio total-energy calculations using a plane-wave basis set. Phys. Rev. B 1996, 54 (16), 11169–11186. DOI: 10.1103/PhysRevB.54.11169.
(45) Kresse, G.; Furthmüller, J. Efficiency of ab-initio total energy calculations for metals and semiconductors using a plane-wave basis set. Computational Materials Science 1996, 6 (1), 15–50. DOI: 10.1016/0927-0256(96)00008-0.
(46) Kresse, G.; Hafner, J. Ab initio molecular dynamics for open-shell transition metals. Phys. Rev. B Condens. Matter 1993, 48 (17), 13115–13118. DOI: 10.1103/physrevb.48.13115.
(47) Steinmann, S. N.; Corminboeuf, C. Comprehensive Benchmarking of a Density-Dependent Dispersion Correction. J. Chem. Theory Comput 2011, 7 (11), 3567–3577. DOI: 10.1021/ct200602x.
(48) Steinmann, S. N.; Corminboeuf, C. A generalized-gradient approximation exchange hole model for dispersion coefficients. J. Chem. Phys. 2011, 134 (4), 44117. DOI: 10.1063/1.3545985.
(49) Monkhorst, H. J.; Pack, J. D. Special points for Brillouin-zone integrations. Phys. Rev. B 1976, 13 (12), 5188–5192. DOI: 10.1103/PhysRevB.13.5188.
(50) Stewart, J. J. P. Optimization of parameters for semiempirical methods VI: more modifications to the NDDO approximations and re-optimization of parameters. J. Mol. Model. 2013, 19 (1), 1–32. DOI: 10.1007/s00894-012-1667-x.
(51) Frisch, M. J.; Trucks, G. W.; Schlegel, H. B.; Scuseria, G. E.; Robb, M. A.; Cheeseman, J. R.; Scalmani, G.; Barone, V.; Petersson, G. A.; Nakatsuji, H. et al. Gaussian 16 Rev. C.01, 2016.
(52) Martínez, L.; Andrade, R.; Birgin, E. G.; Martínez, J. M. PACKMOL: A package for building initial configurations for molecular dynamics simulations. J. Comput. Chem.2009, 30 (13), 2157–2164. DOI: 10.1002/jcc.21224.
(53) Neese, F. (2012) The ORCA program system, Wiley Interdiscip. Rev.: Comput. Mol. Sci., 2, 73-78.
(54) Steinmann, S. N.; Michel, C. How to Gain Atomistic Insights on Reactions at the Water/Solid Interface?. ACS Catal. 2022, 12, 6294– 6301, DOI: 10.1021/acscatal.2c00594
(55) Steinmann, S. N.; Hermawan, A.; Bin Jassar, M.; Seh, Z. W. Autonomous high-throughput computations in catalysis. Chem Cat. 2022, 2 (5), 940–956. DOI: 10.1016/j.checat.2022.02.009.
(56) Liu, Q.; Li, S.; Wang, S.; Zhang, X.; Zhou, S.; Bai, Y.; Zheng, J.; Lu, X. Kinetically Determined Phase Transition from Stage II (LiC12) to Stage I (LiC6) in a Graphite Anode for Li-Ion Batteries. J. Phys. Chem. Lett. 2018, 9 (18), 5567–5573. DOI: 10.1021/acs.jpclett.8b02750.

(57) Lenchuk, O.; Adelhelm, P.; Mollenhauer, D. Comparative study of density functionals for the description of lithium-graphite intercalation compounds. J. Comput. Chem. 2019, 40 (27), 2400–2412. DOI: 10.1002/jcc.26017.
(58) Staub, R.; Steinmann, S. N. Parameter-Free Coordination Numbers for Solutions and Interfaces. J. Chem. Phys. 2020, 152 (2), 024124. DOI: 10.1063/1.5135696.
(59) Bertolini, S.; Balbuena, P. B. Effect of solid electrolyte interphase on the reactivity of polysulfide over lithium-metal anode. Electrochim. Acta 2017, 258, 1320–1328. DOI: 10.1016/j.electacta.2017.11.190.

Graphical Abstract

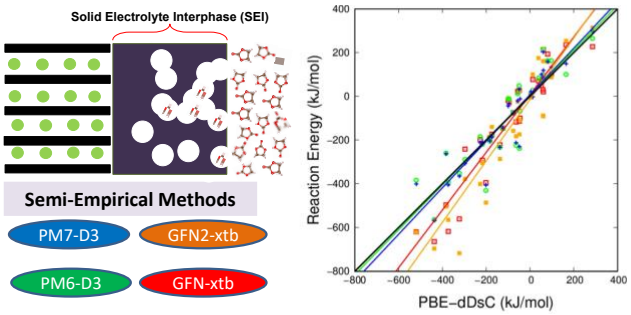
Solid Electrolyte Interphase (SEI)
Semi-Empirical Methods
PM7-D3
GFN2-xtb
PM6-D3
GFN-xtb
Reaction Energy (kJ/mol)
PBE–dDsC (kJ/mol)
400
200
0
-200
-400
-600
-800
-800
-600
-400
-200
0
200
400